FEBS Letters 589 (2015) 3247–3253

FEBS Letters

journal homepage: www.FEBSLetters.org

# Crystal structure of human nuclear pore complex component NUP43

Chao Xu [a,b], Zhihong Li [a], Hao He [a], Amy Wernimont [a], Yanjun Li [a], Peter Loppnau [a], Jinrong Min [a,c,*]

[a] Structural Genomics Consortium, University of Toronto, 101 College St., Toronto, Ontario M5G 1L7, Canada
[b] Hefei National Laboratory for Physical Sciences at Microscale and School of Life Sciences, University of Science and Technology of China, Hefei, Anhui 230027, People's Republic of China
[c] Department of Physiology, University of Toronto, Toronto, Ontario M5S 1A8, Canada

ARTICLE INFO

*Article history:*
Received 24 July 2015
Revised 29 August 2015
Accepted 8 September 2015
Available online 29 September 2015

Edited by Christian Griesinger

*Keywords:*
Nup107 subcomplex
Nup43
Nup85
Seh1L
WD40 repeat

ABSTRACT

**Nuclear pore complexes (NPC) form nuclear pores that cross the nuclear envelope and allow molecules to transport between the nucleus and the cytoplasm. We solved the crystal structure of human Nup43 (hNUP43), an important component in the Nup107 subcomplex of NPC. hNup43 adopts a seven-bladed β-propeller fold. We confirmed by ITC that neither human Nup37 (hNup37) nor human Nup133 (hNup133) interacts with hNup43. We demonstrated by analytical gel filtration that the human Nup85-Seh1L binary complex recruits hNup43 to form a ternary complex. Based on amino acid sequence analysis, we predicted the hNup85-hSeh1L binding surface of hNup43.**


## 1. Introduction

In eukaryotic cells, the nuclear envelope separates the nucleus from the cytoplasm and controls traffic between both, such as the transport of mRNAs and ribosomal proteins [1,2]. During cell mitosis, the nuclear envelope disassembles completely, and reassembles step by step at the end of mitosis. The nuclear pore complex (NPC), which is formed by several sub complexes, is embedded into the nuclear envelope [3–5]. The components of the mammalian NPC were identified and proteomically analyzed in 2002 [3].

One of the most studied Nup subcomplex is the Nup107 subcomplex. The Nup107 subcomplex not only facilitates the reassembly of the nuclear envelope following mitosis, but also regulates eukaryotic gene expression and heterochromatin in epigenetics [6]. The yeast Nup107 subcomplex consists of Nup85, Nup145C, Nup84, Nup133, Nup120, Seh1 and Sec13, whereas the human Nup107 subcomplex contains two additional components: Nup37 and Nup43 [7,8].

In the past few years, the atomic structures of several eukaryotic Nup107 components have been determined [9], such as Nup133N-terminal domain [10], the Nup133 C-terminal domain in complex with Nup107 C-terminal domain [11], the Nup85–Seh1 complex [12,13], the Sec13–Nup145C heterodimer [14], the Sec13–Nup145C–Nup84 heterotrimer [15,16], Nup120 N-terminal domain [17,18], Nup37–Nup120 [19], the Nup145C–Nup120-central triskelion [20], and the intact complex only lacking Nup133 [9]. Recently, the low-resolution structure of the human Nup107 subcomplex within the NPC scaffold was also determined by Cryo-electron microscopy (Cryo-EM) [21]. The Nup107 subcomplex adopts the Y-shape, which is evolutionarily conserved as visualized by negative stain EM and Nup43 is a unique component in higher eukaryotes [21–23]. Overall Nup107 subcomplex is arranged in NPC in two sixteen-membered double rings at the cytoplasmic and nuclear side of the nuclear envelope in a horizontal orientation [9,21]. However, lack of high-resolution structural information for remaining components still hampers elucidation of Nup107 molecular function. Nup43, a WD40 containing protein, is conserved in higher eukaryotes, but absent in the yeast Nup107 subcomplex. Our exploration of hNup43 structure will help to explain aspects of nuclear pore biology unique to higher eukaryotes.

*Author contributions:* C.X. and J.M. conceived the project. C.X. performed the experiments and analyzed the data. Z.H. assisted in purification of the hNup43. H.H. cultured the cell. A.W. assisted in refining the structure of hNup43. P.L. and Y.L. cloned the constructs of Nup43, Nup37, Nup133, Seh1L and Nup85. J.M. supervised the project.

* Corresponding author at: Structural Genomics Consortium, University of Toronto, 101 College St., Toronto, Ontario M5G 1L7, Canada.
*E-mail address:* jr.min@utoronto.ca (J. Min).

http://dx.doi.org/10.1016/j.febslet.2015.09.008
0014-5793/

Here we present the crystal structure of full length hNup43 (human Nup43). As predicted, Nup43 adopts a canonical WD40 fold similar to other members of the family. We also purified full length human proteins human Nup37 (hNup37) and human Nup133 (hNup133), and found that neither interacts with hNup43. In contrast, the human Nup85–Seh1L complex (hNup85–hSeh1L), which we also purified, did form a ternary complex with hNup43. Based on amino acid sequence alignment of Nup43 orthologs, we predicted the hNup85–hSeh1 binding site of hNup43.

## 2. Results and discussion

In our hands, hNup43 was not soluble in an *E. coli* expression system. Thus we cloned hNup43 into a Baculovirus vector and expressed it in SF9 insect cells. Following purification and crystallization of full length hNup43, we determined its crystal structure at a resolution of 1.75 Å. Crystallographic statistics are summarized in Table 1. The current crystallographic model omits some N-terminal and loop-region amino acid residues that were poorly resolved in the electron density maps and are presumed disordered in the crystal.

As shown in Fig. 1A and B, hNup43 adopts a canonical β-propeller fold, consisting of seven WD40 repeats (13–73, 77–116, 134–168, 175–212, 220–257, 264–344, 353–380 plus 5–8) and each WD40 repeat of Nup43 is composed of four anti-parallel β strands, resembling other WD40 containing proteins, such as WDR5, WDR61 and EED [24–26]. (Fig. 1A and B). There are two molecules of hNup43 in the asymmetric unit and the global RMSD (Root Mean Square Deviation) between back bones of the two molecules is only 0.2 Å. Most of residues in the two molecules are visible. However, residues Met1-Glu3, Phe52-Phe61, Gly123-Y129, Thr293-Ser328, and Thr333-Asp338 are invisible in both molecules in the same asymmetric unit. In contrast, Gly50 and Asp51 are missing in only one molecule and Arg339 is missing in the other molecule. All of the missing residues lie either in the terminus or in loop regions, and they are invisible presumably due to the flexibility of these regions. Slight structural deviations come from flexible loop regions. The only exception comes from Glu62–Gln66, which include the very beginning of β1D (Fig. 1A and B). Probably these four residues also have internal flexibility because they immediately follow the invisible loop Phe52–Phe61 (Fig. 1A and B).

**Table 1**
Data collection and refinement statistics.

| Data | hNUP43 (1–380) |
|---|---|
| Wavelength [Å] | 0.9795 |
| Space group | $P2_12_12$ |
| Unit cell *a*, *b*, *c* [Å] | 80.74, 161.96, 58.20 |
| Resolution (outer shell) [Å] | 47.26–1.75 (1.84–1.75) |
| Unique observed HKLs | 77,846 (11,224) |
| Completeness [%] | 100.0 (100.0) |
| Redundancy | 7.4 (7.4) |
| $R_{merge}$ [%] | 7.8 (94.0) |
| $R_{PIM}$ [%] | 3.1 (37.0) |
| Mean ($I/\sigma_I$) | 15.8 (2.2) |
| Refinement data resolution | 45.00–1.75 |
| HKLs used/free (%) | 75,293/2490 (3.3%) |
| $R_{cryst}/R_{free}$ [%] | 18.1/21.3 |
| Number of atoms/average B [Å$^2$] (not including unidentified atoms/ions) | 5412/29.1 |
| Protein | 5134/28.9 |
| Water | 278/33.4 |
| RMSDs bonds [Å]/angles [°] | 0.016/1.5 |
| Residues in Ramachandran plot[a]: residues in favored region/allowed/outlier regions [38] [%] | 97.1/2.9/0 |
| PDB code | 4I79 |

[a] Molprobity 4.1–537. The highest resolution shell is shown in parentheses.

According to the recently published cryo-EM structure of Y-shape hNup107 subcomplex, hNup43 bind to hNup85 via its bottom surface and is close to hNup37 [21]. To investigate the interactions of hNup43 with other components within the hNup107 subcomplex, we purified full length hNup85–hSeh1L complex, hNup37 and hNup133 to test if either of them binds to hNup43. We mixed hNup85–hSeh1L and hNup43 in a molecular ratio of 1:1.5 and purified them via gel filtration on a Superdex 200 (Fig. 2A). As shown in Fig. 2A, one peak appeared at a molecular weight ~160kDa. Bio-Rad's gel filtration standard is used in the same buffer to estimate the molecular weight and size. As a control, the hNup85–hSeh1L binary complex appeared at a molecular weight of roughly ~110kDa (Fig. 2B). The gel filtration assay indicated the formation of hNup43–hNup85–hSeh1L ternary complex in a molecular ratio of 1:1:1.

In addition, we also used isothermal titration calorimetry (ITC) to test if hNup37 or hNup133 binds to hNup43 and found neither of them interacts with hNup43 directly (Fig. 2C and D). Overall, our in vitro binding data is well consistent with the cryo-EM structure of the hNup107 complex and further confirmed the direct interaction between hNup43 and hNup85–hSeh1L.

To date, many WD40 protein complexes were solved with ligand bound to the top or bottom surface of the WD40 repeats. We compared the structure of hNup43 with other solved WD40 proteins of the Nup107 subcomplex, such as yeast Nup37–Nup120 (4GQ2), yeast Sec13–Nup145C complex (3JRP), yeast Nup85–Seh1complex (3EWE) and human Nup133 (1XKS) (Fig. 3). hNup43, Nup37 and hNup133 all contain seven WD40 repeats (Fig. 3A, D and E), whereas Seh1 and Sec13 contains six WD40 repeats (Fig. 3B and C). In Fig. 3B and C, the beta strands of Nup85 and Nup145C are inserted into the six-bladed propellers of Seh1 and Sec13, respectively, as the seventh blade. In Fig. 3D, Nup37 mainly contacts Nup120 through its top surface, the insertion fragments on one side also contribute to the interaction. In contrast, hNup43 interacts with hNup85 via the bottom of the WD40 repeats in the cryo-EM structure of the Nup107 [21].

Nup43 exists in various species, which prompts us to analyze the sequence conservation between them [27]. As shown in Fig. S1, the WD40 repeats of Nup43 are highly conserved in other eukaryotic organisms. We showed the surface representation of conservation in three perspectives according to the sequence alignment (Fig. S2). In the cryo-EM structure, hNup43 interacts with hNup85 via its bottom surface. Since the conserved residues distributed extensively at the bottom surface, it is difficult to map exactly the binding site and we could not exclude the possibility that hNup85–hSeh1L may bind to hNup43 via an extensive surface at the bottom.

At the bottom of the hNup43 WD40 repeats, there are one long loop (resi 291–340) between β6C and β6D. Most of the loop residues are invisible and the length of the loop varies among Nup43 orthologs. In contrast, another loop between β1A and β1B (resi 19–30), exhibits an ordered conformation in the crystal structure. It is solvent accessible and protrudes at the bottom surface which might allow it to contact the helix region of hNup85, as implied by the cryo-EM structure of Nup107 complex (Fig. 1B and D).

In contrast to the bottom surface, conserved residues at the top surface are more convergent. In 2012, Wu et al. performed a detailed bioinformatics analysis on known WD40-repeat containing structures, predicting the potential ligand binding residues on the top face of WD40 repeats [28]. Accordingly, we analyzed the β-bulge formed in each WD40 repeat. As shown in Fig. 4A, Gly35 formed three backbone hydrogen bonds with Ser14 and Lys15 in

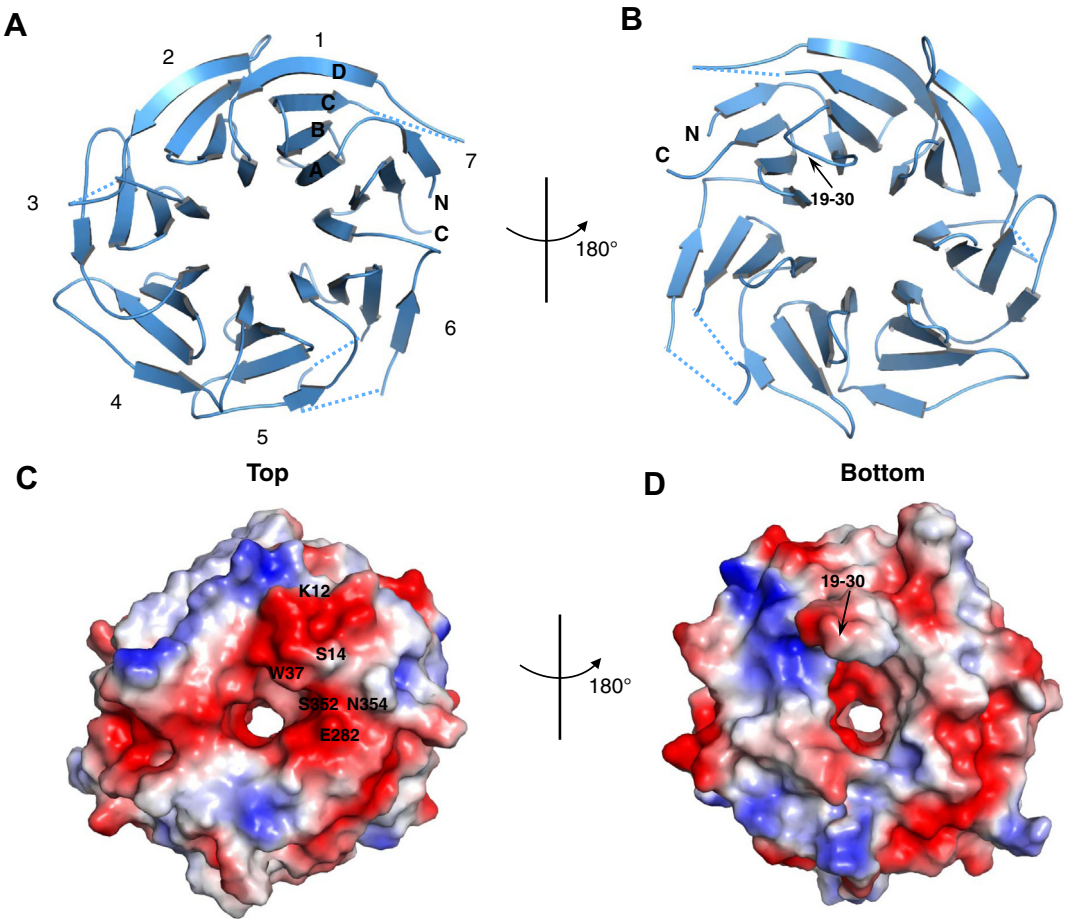


**Fig. 1.** Crystal structure of hNup43. (A) Top and (B) bottom view of hNup43 shown in blue cartoon. (C) Top and (D) bottom view of the electrostatic surface of hNup43. Missing loop regions are shown as dashed dotted lines.

the first WD40 repeat. Next we identified residues at $R_1$, $R_1$-2 or D-1 positions of each WD40 repeat, excluding buried residues. Taken together with the sequence conservation, we identified a cluster of residues in WD1, WD6 and WD7 as the potential binding patches, which are also consistent with the conserved residues shown in (Figs. S2 and 4B). However, we could not exclude the possibility that Nup43 might contact other components of Nup107 subcomplex via the other surfaces.

Previous reports identified Nup proteins could interact with nucleic acids. As shown in Fig. 1C, the electrostatic surface of Nup43 (top view) exhibits extensive negatively charged regions. It would be implausible for this highly negative surface of Nup43 to interact with DNA or RNA, although hNup43 may also interact with nucleic acids via other partners in its Nup107 subcomplex.

## 3. Conclusion

Here we present the high resolution crystal structure of full length Nup43, which adopted a seven bladed β-propeller fold. We analyzed the interaction of Nup43 with other components of the Nup107 subcomplex, hNup37, hNup133, and hNup85–hSeh1L complex and found that Nup43 interacts with hNup85–hSeh1L, but not hNup37 or hNup133, to form a ternary complex. Inspired by the existing cryo-EM structure, we identified an ordered loop at the bottom surface of hNup43 WD40 that may directly bind to hNup85–hSeh1L. In addition, we also identified a cluster of conserved residues on the top face of Nup43 WD40 repeats that potentially play an important role in recognizing unknown ligands. Future structural investigation of Nup43 with Nup85–Seh1L would be required to understand the molecular details.

## 4. Materials and methods

### 4.1. Protein expression and purification

The hNup43 (1–380) cDNA was subcloned into the pFBOH-lic vector and expressed in Sf9 insect cells. 0.8 l of Sf9 cells were infected with 8 ml of P3 recombinant baculovirus, and grown in a 2.8 L shaker flask at 27 °C and 100 rpm with HyQ® SFX-insect serum medium containing Gentamicin (10 μg/ml). Infected cells were harvested when viability dropped to 80–85%, normally after 48 h. Harvested cells were washed with cold PBS buffer, and then flash frozen in liquid nitrogen and stored at −80 °C for purification. Recombinant hNup43 containing an N-terminal 6×His tag was purified on a Ni–NTA resin (Qiagen) and further purified on a Superdex 200 gel filtration column (GE Healthcare, Tyrone, PA) in a buffer containing 20 mM Tris–HCl pH 7.5, 150 mM NaCl and 1 mM dithiothreitol. Purified Nup43 protein was concentrated to 15 mg/ml and stored at −80 °C before further use.

cDNAs of the full length hNup37 (1–326), hNup133 (1–1156), hNup85 (1–656) and hSeh1L (1–360) were also subcloned into the pFBOH-lic vector. hNup37 and hNup133 were expressed in Sf9 insect cells separately, whereas hNup85 (1–656) and hSeh1L (1–360) were co-infected and expressed in Sf9 insect cells to form hNup85–hSeh1L complex. They were purified with similar methods to those mentioned above.

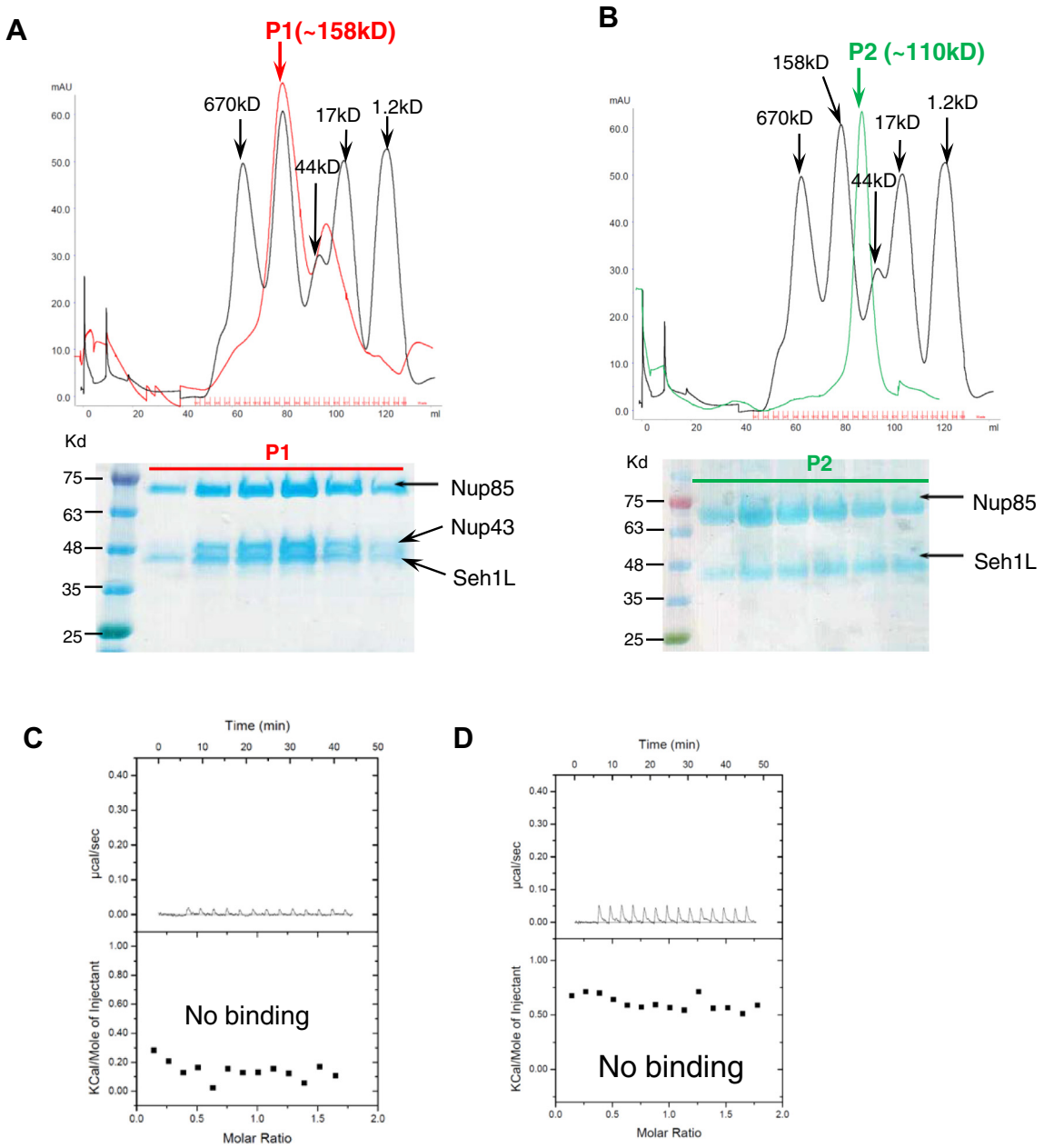


**Fig. 2.** The interaction of hNup43 with other components of Nup197 subcomplex. (A) The purified hNup43 was mixed with the hNup85–hSeh1L complex in a molecular ratio of 1.5:1 and the mixture was purified by an analytical gel filtration column Superdex 200 (red curve). Bio-rad protein standards were used in the same condition to estimate the molecular weight (black curve). The Coomassie blue staining SDS gel of the purified ternary complex (peak P1). (B) The hNup85–hSeh1L complex was purified by an analytical gel filtration column Superdex 200 (green curve) and its molecular weight was estimated with the same protein standards as shown in Fig. 2A. The Coomassie blue staining SDS gel of the purified ternary complex (peak P2). (C) ITC binding curve of hNup43 with hNup37. (D) ITC binding curve of hNup43 with hNup133.

hNup37 and hNup133 were concentrated to 10 mg/ml and 15 mg/ml and stocks stored at −80 °C after purification by Superdex 200 gel filtration column in a buffer containing 20 mM Tris–HCl pH 7.5, 150 mM NaCl and 1 mM DTT. hNup85–hSeh1L complex were purified by gel filtration in a buffer containing 20 mM Tris–HCl pH 7.5, 400 mM NaCl and 1 mM DTT. The peak of the heterodimer were harvested and mixed with hNup43 in a molecular ratio of 1:1.5 and further purified by a Superdex 200 gel filtration assay with the buffer containing 20 mM Tris–HCl pH 7.5, 400 mM NaCl and 1 mM DTT. The peaks of the curve were collected, pooled and analyzed by SDS–PAGE. The Bio-Rad protein standards are dissolved and analyzed in the same condition to determine the molecular weights of the hNup85–hSeh1L complex and the hNup43–hNup85–hSeh1L complex. The yields of Nup43 and hNup85–hSeh1L heterodimer are 5 mg from 8 L of media and 2 mg from 8 L of media, respectively.

### 4.2. Crystallization

Purified full length hNup43 was crystallized at 18 °C using the sitting drop vapor diffusion method. Diffracting crystals appeared in the crystallization buffer containing 25% PEG-3350, 0.1 M ammonium sulfate, 0.1 M sodium HEPES, pH 7.5. The protein was mixed with the crystallization buffer in a 1:1 ratio (1 µl protein mixed with 1 µl crystallization buffer). Before freezing in liquid nitrogen, the crystals were immersed into a mixture consisting of reservoir solution plus 10% glycerol (v/v).

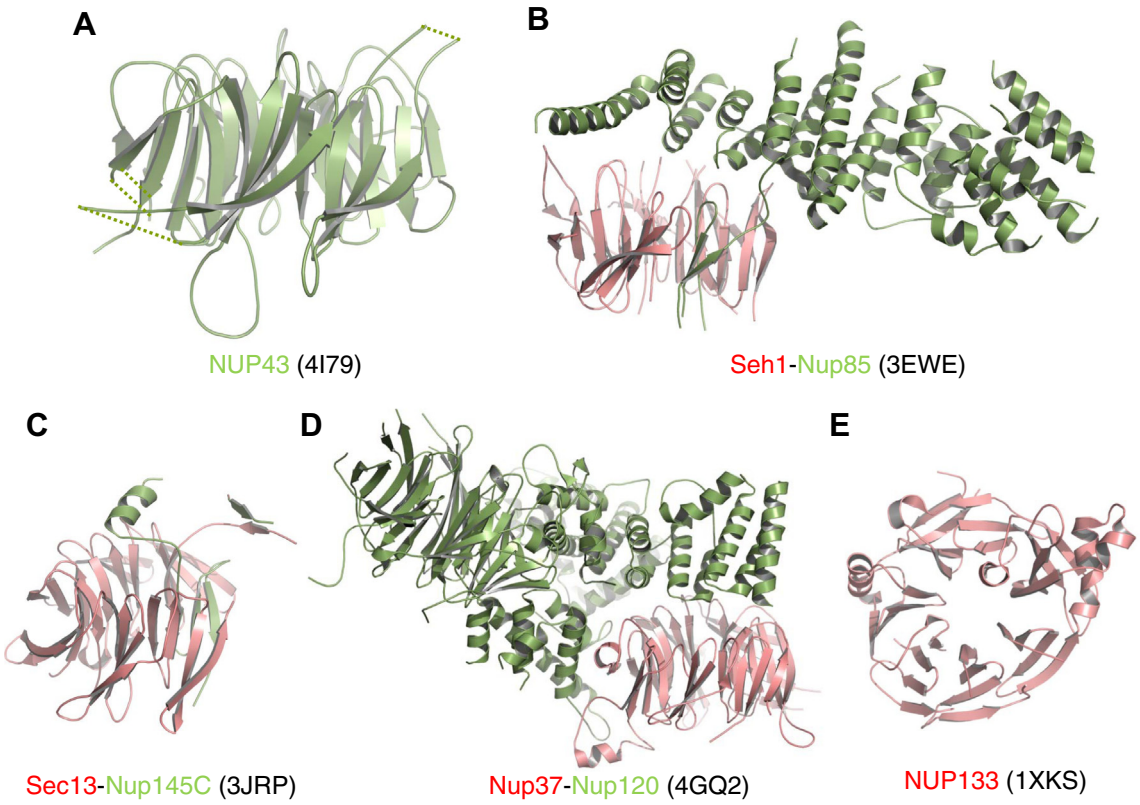


**Fig. 3.** Structures of WD40 proteins of the Nup107 subcomplex. All WD40 proteins are shown in green and their binding partners are shown in red. (A) hNup43 (4I79); (B) yeast Nup85–Seh1 (3EWE); (C) Sec13–Nup145C (3JRP); (D) Nup37–Nup120 (4GQ2); (E) Nup133 WD40 repeats (1XKS).

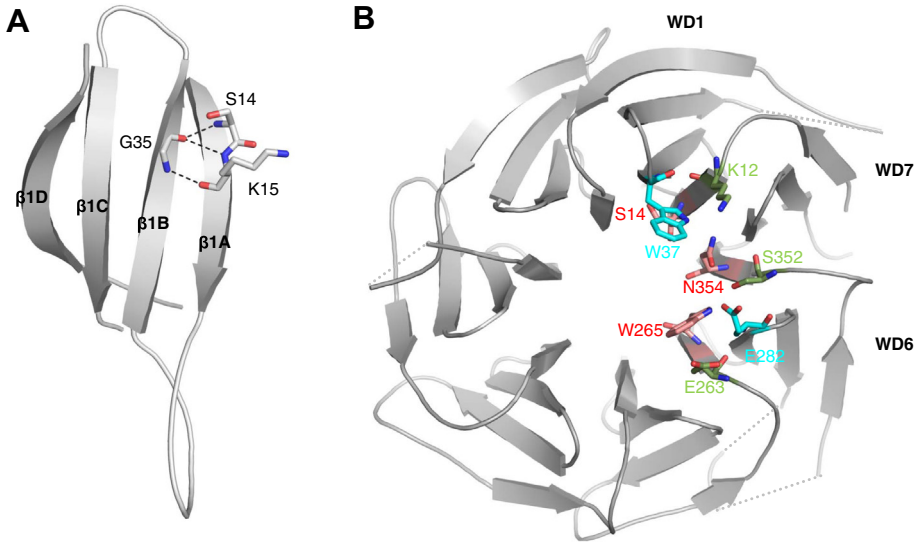


**Fig. 4.** The potential binding site on top face of Nup43 WD40 repeats. (A) The β-bulge formed between β1A and β1B. The first WD40 repeat is shown in gray cartoon and the residues involved in the hydrogen bonds are shown in sticks. (B) The overall structure of Nup43 is shown in gray cartoon from top view, the same orientation as the one in Fig. 1A. The potential binding pocket is formed by conserved residues at $R_1$, $R_1$-2 and D-1 positions, which are shown in red, green and cyan sticks, respectively. The analysis was performed according to the presented method by Wu et al. [28].

### *4.3. Data collection, structure determination, structure refinement and data deposition*

A continuous set of 180 single-degree oscillation images was collected at beam line 08 ID at the Canadian Light Source [29]. Data were reduced with the program XDS [30] and scaled with POINTLESS/SCALA [31]. The crystal structure was solved by molecular replacement with the program PHASER [32] and an ensemble of FFAS03 [33]/SCWRL [34] models derived from Protein Data Bank [35] entries 2XZM [36] (chain R), 3CFS [37], and 4AOW [38]. PHENIX simulated annealing refinement with slow cooling from a starting temperature of "10,000" was followed by ARP/WARP atom update [39], automated model building [40] and iterations of rebuilding with the program COOT [41], refinement with REFMAC

[42] and geometry evaluation on the MOLPROBITY [43] server. The final structure has been deposited into Protein Data Bank (PDB) with accession code 4I79.

### 4.4. Isothermal titration calorimetry (ITC) binding experiments

ITC measurements were performed at 25 °C with a VP-ITC micro calorimeter (MicroCal Inc.) as described previously [44]. The experiments were recorded by injecting 10 μl of hNup43 (400 μM) into a sample cell containing 20 μM hNup37 or hNup133 in 20 mM Tris–HCl (pH 7.5) and 150 mM NaCl. All proteins were dialyzed in the same buffer before the binding experiments. The concentrations of proteins were estimated with absorbance spectroscopy using their extinction coefficients at 280 nm. A total of 13–14 injections were performed with a spacing of 180 s and a reference power of 15 μcal/s. Binding isotherms were plotted and analyzed with Origin Software (MicroCal Inc.).

## Acknowledgement

We thank Dr. Wolfram Tempel for the work in data collection and structure determination of hNup43. The SGC is a registered charity (No. 1097737) that receives funds from AbbVie, Bayer Pharma AG, Boehringer Ingelheim, Canada Foundation for Innovation, Eshelman Institute for Innovation, Genome Canada, Innovative Medicines Initiative (EU/EFPIA) [ULTRA-DD Grant No. 115766], Janssen, Merck & Co., Novartis Pharma AG, Ontario Ministry of Economic Development and Innovation, Pfizer, São Paulo Research Foundation-FAPESP, Takeda, and the Wellcome Trust. This work was also supported by Grants from the National Natural Science Foundation of China (NSFC) (31570737).

## Appendix A. Supplementary data

Supplementary data associated with this article can be found, in the online version, at http://dx.doi.org/10.1016/j.febslet.2015.09.008.

## References

[1] Strambio-De-Castillia, C., Niepel, M. and Rout, M.P. (2010) The nuclear pore complex: bridging nuclear transport and gene regulation. Nat. Rev. Mol. Cell Biol. 11, 490–501.
[2] Cook, A., Bono, F., Jinek, M. and Conti, E. (2007) Structural biology of nucleocytoplasmic transport. Annu. Rev. Biochem. 76, 647–671.
[3] Cronshaw, J.M., Krutchinsky, A.N., Zhang, W., Chait, B.T. and Matunis, M.J. (2002) Proteomic analysis of the mammalian nuclear pore complex. J. Cell Biol. 158, 915–927.
[4] Schwartz, T.U. (2005) Modularity within the architecture of the nuclear pore complex. Curr. Opin. Struct. Biol. 15, 221–226.
[5] Lim, R.Y. and Fahrenkrog, B. (2006) The nuclear pore complex up close. Curr. Opin. Cell Biol. 18, 342–347.
[6] Walther, T.C., Alves, A., Pickersgill, H., Loiodice, I., Hetzer, M., Galy, V., Hulsmann, B.B., Kocher, T., Wilm, M., Allen, T., Mattaj, I.W. and Doye, V. (2003) The conserved Nup107–160 complex is critical for nuclear pore complex assembly. Cell 113, 195–206.
[7] Gonzalez-Aguilera, C. and Askjaer, P. (2012) Dissecting the NUP107 complex: multiple components and even more functions. Nucleus 3, 340–348.
[8] Loiodice, I., Alves, A., Rabut, G., Van Overbeek, M., Ellenberg, J., Sibarita, J.B. and Doye, V. (2004) The entire Nup107-160 complex, including three new members, is targeted as one entity to kinetochores in mitosis. Mol. Biol. Cell 15, 3333–3344.
[9] Stuwe, T., Correia, A.R., Lin, D.H., Paduch, M., Lu, V.T., Kossiakoff, A.A. and Hoelz, A. (2015) Nuclear pores. Architecture of the nuclear pore complex coat. Science 347, 1148–1152.
[10] Berke, I.C., Boehmer, T., Blobel, G. and Schwartz, T.U. (2004) Structural and functional analysis of Nup133 domains reveals modular building blocks of the nuclear pore complex. J. Cell Biol. 167, 591–597.
[11] Boehmer, T., Jeudy, S., Berke, I.C. and Schwartz, T.U. (2008) Structural and functional studies of Nup107/Nup133 interaction and its implications for the architecture of the nuclear pore complex. Mol. Cell 30, 721–731.
[12] Brohawn, S.G., Leksa, N.C., Spear, E.D., Rajashankar, K.R. and Schwartz, T.U. (2008) Structural evidence for common ancestry of the nuclear pore complex and vesicle coats. Science 322, 1369–1373.
[13] Debler, E.W., Ma, Y., Seo, H.S., Hsia, K.C., Noriega, T.R., Blobel, G. and Hoelz, A. (2008) A fence-like coat for the nuclear pore membrane. Mol. Cell 32, 815–826.
[14] Hsia, K.C., Stavropoulos, P., Blobel, G. and Hoelz, A. (2007) Architecture of a coat for the nuclear pore membrane. Cell 131, 1313–1326.
[15] Brohawn, S.G. and Schwartz, T.U. (2009) Molecular architecture of the Nup84–Nup145C–Sec13 edge element in the nuclear pore complex lattice. Nat. Struct. Mol. Biol. 16, 1173–1177.
[16] Nagy, V., Hsia, K.C., Debler, E.W., Kampmann, M., Davenport, A.M., Blobel, G. and Hoelz, A. (2009) Structure of a trimeric nucleoporin complex reveals alternate oligomerization states. Proc. Natl. Acad. Sci. USA 106, 17693–17698.
[17] Seo, H.S., Ma, Y., Debler, E.W., Wacker, D., Kutik, S., Blobel, G. and Hoelz, A. (2009) Structural and functional analysis of Nup120 suggests ring formation of the Nup84 complex. Proc. Natl. Acad. Sci. USA 106, 14281–14286.
[18] Leksa, N.C., Brohawn, S.G. and Schwartz, T.U. (2009) The structure of the scaffold nucleoporin Nup120 reveals a new and unexpected domain architecture. Structure 17, 1082–1091.
[19] Liu, X., Mitchell, J.M., Wozniak, R.W., Blobel, G. and Fan, J. (2012) Structural evolution of the membrane-coating module of the nuclear pore complex. Proc. Natl. Acad. Sci. USA 109, 16498–16503.
[20] Kelley, K., Knockenhauer, K.E., Kabachinski, G. and Schwartz, T.U. (2015) Atomic structure of the Y complex of the nuclear pore. Nat. Struct. Mol. Biol. 22, 425–431.
[21] Bui, K.H., von Appen, A., DiGuilio, A.L., Ori, A., Sparks, L., Mackmull, M.T., Bock, T., Hagen, W., Andres-Pons, A., Glavy, J.S. and Beck, M. (2013) Integrated structural analysis of the human nuclear pore complex scaffold. Cell 155, 1233–1243.
[22] Thierbach, K., von Appen, A., Thoms, M., Beck, M., Flemming, D. and Hurt, E. (2013) Protein interfaces of the conserved Nup84 complex from *Chaetomium thermophilum* shown by crosslinking mass spectrometry and electron microscopy. Structure 21, 1672–1682.
[23] Lutzmann, M., Kunze, R., Buerer, A., Aebi, U. and Hurt, E. (2002) Modular self-assembly of a Y-shaped multiprotein complex from seven nucleoporins. EMBO J. 21, 387–397.
[24] Xu, C. and Min, J. (2011) Structure and function of WD40 domain proteins. Protein Cell 2, 202–214.
[25] Xu, C., Bian, C., Yang, W., Galka, M., Ouyang, H., Chen, C., Qiu, W., Liu, H., Jones, A.E., MacKenzie, F., Pan, P., Li, S.S., Wang, H. and Min, J. (2010) Binding of different histone marks differentially regulates the activity and specificity of polycomb repressive complex 2 (PRC2). Proc. Natl. Acad. Sci. USA 107, 19266–19271.
[26] Schuetz, A., Allali-Hassani, A., Martin, F., Loppnau, P., Vedadi, M., Bochkarev, A., Plotnikov, A.N., Arrowsmith, C.H. and Min, J. (2006) Structural basis for molecular recognition and presentation of histone H3 by WDR5. EMBO J. 25, 4245–4252.
[27] Neumann, N., Lundin, D. and Poole, A.M. (2010) Comparative genomic evidence for a complete nuclear pore complex in the last eukaryotic common ancestor. PLoS One 5, e13241.
[28] Wu, X.H., Wang, Y., Zhuo, Z., Jiang, F. and Wu, Y.D. (2012) Identifying the hotspots on the top faces of WD40-repeat proteins from their primary sequences by beta-bulges and DHSW tetrads. PLoS One 7, e43005.
[29] Grochulski, P., Fodje, M.N., Gorin, J., Labiuk, S.L. and Berg, R. (2011) Beamline 08ID-1, the prime beamline of the Canadian macromolecular crystallography facility. J. Synchrotron Radiat. 18, 681–684.
[30] Kabsch, W. (2010) XDS. Acta Crystallogr. D Biol. Crystallogr. 66, 125–132.
[31] Evans, P.R. (2011) An introduction to data reduction: space-group determination, scaling and intensity statistics. Acta Crystallogr. D Biol. Crystallogr. 67, 282–292.
[32] McCoy, A.J., Grosse-Kunstleve, R.W., Adams, P.D., Winn, M.D., Storoni, L.C. and Read, R.J. (2007) Phaser crystallographic software. J. Appl. Crystallogr. 40, 658–674.
[33] Jaroszewski, L., Rychlewski, L., Li, Z., Li, W. and Godzik, A. (2005) FFAS03: a server for profile–profile sequence alignments. Nucleic Acids Res. 33, W284–W288.
[34] Canutescu, A.A., Shelenkov, A.A. and Dunbrack Jr., R.L. (2003) A graph-theory algorithm for rapid protein side-chain prediction. Protein Sci. 12, 2001–2014.
[35] Berman, H.M., Westbrook, J., Feng, Z., Gilliland, G., Bhat, T.N., Weissig, H., Shindyalov, I.N. and Bourne, P.E. (2000) The protein data bank. Nucleic Acids Res. 28, 235–242.
[36] Rabl, J., Leibundgut, M., Ataide, S.F., Haag, A. and Ban, N. (2011) Crystal structure of the eukaryotic 40S ribosomal subunit in complex with initiation factor 1. Science 331, 730–736.
[37] Murzina, N.V., Pei, X.Y., Zhang, W., Sparkes, M., Vicente-Garcia, J., Pratap, J.V., McLaughlin, S.H., Ben-Shahar, T.R., Verreault, A., Luisi, B.F. and Laue, E.D. (2008) Structural basis for the recognition of histone H4 by the histone-chaperone RbAp46. Structure 16, 1077–1085.
[38] Ruiz Carrillo, D., Chandrasekaran, R., Nilsson, M., Cornvik, T., Liew, C.W., Tan, S. M. and Lescar, J. (2012) Structure of human Rack1 protein at a resolution of 2.45 A. Acta Crystallogr. Sect. F: Struct. Biol. Cryst. Commun. 68, 867–872.
[39] Perrakis, A., Sixma, T.K., Wilson, K.S. and Lamzin, V.S. (1997) WARP: improvement and extension of crystallographic phases by weighted averaging of multiple-refined dummy atomic models. Acta Crystallogr. D Biol. Crystallogr. 53, 448–455.
[40] Langer, G., Cohen, S.X., Lamzin, V.S. and Perrakis, A. (2008) Automated macromolecular model building for X-ray crystallography using ARP/wARP version 7. Nat. Protoc. 3, 1171–1179.

[41] Emsley, P., Lohkamp, B., Scott, W.G. and Cowtan, K. (2010) Features and development of coot. Acta Crystallogr. D Biol. Crystallogr. 66, 486–501.
[42] Murshudov, G.N., Skubak, P., Lebedev, A.A., Pannu, N.S., Steiner, R.A., Nicholls, R.A., Winn, M.D., Long, F. and Vagin, A.A. (2011) REFMAC5 for the refinement of macromolecular crystal structures. Acta Crystallogr. D Biol. Crystallogr. 67, 355–367.
[43] Chen, V.B., Arendall 3rd, W.B., Headd, J.J., Keedy, D.A., Immormino, R.M., Kapral, G.J., Murray, L.W., Richardson, J.S. and Richardson, D.C. (2010) MolProbity: all-atom structure validation for macromolecular crystallography. Acta Crystallogr. D Biol. Crystallogr. 66, 12–21.
[44] Xu, C., Bian, C., Lam, R., Dong, A. and Min, J. (2011) The structural basis for selective binding of non-methylated CpG islands by the CFP1 CXXC domain. Nat. Commun. 2, 227.